Li *et al.*
Chinese Journal of Mechanical Engineering (2022) 35:108
https://doi.org/10.1186/s10033-022-00782-5

Chinese Journal of Mechanical Engineering

ORIGINAL ARTICLE

Open Access

Wheel Setting Error Modeling and Compensation for Arc Envelope Grinding of Large-Aperture Aspherical Optics

Changsheng Li[1,2], Lin Sun[1,2*], Zhaoxiang Chen[1], Jianfang Chen[3], Qijing Lin[1,2], Jianjun Ding[1,2] and Zhuangde Jiang[1,2]

Abstract

Precision grinding is a key process for realizing the use of large-aperture aspherical optical elements in laser nuclear fusion devices, large-aperture astronomical telescopes, and high-resolution space cameras. In this study, the arc envelope grinding process of large-aperture aspherical optics is investigated using a CM1500 precision grinding machine with a maximum machinable diameter of Φ1500 mm. The form error of the aspherical workpiece induced by wheel setting errors is analytically modeled for both parallel and cross grinding. Results show that the form error is more sensitive to the wheel setting error along the feed direction than that along the lateral direction. It is a bilinear function of the feed-direction wheel setting error and the distance to the optical axis. Based on the error function above, a method to determine the wheel setting error is proposed. Subsequently, grinding tests are performed with the wheels aligned accurately. Using a newly proposed partial error compensation method with an appropriate compensation factor, a form error of 3.4 μm peak-to-valley (PV) for a Φ400 mm elliptical K9 glass surface is achieved.

Keywords: Aspherical optics, Wheel setting, Arc envelope grinding, Form error, Large aperture

1 Introduction

Large ultra-precision aspheric optical elements are highly demanded for the development of laser nuclear fusion devices [1], large-aperture astronomical telescopes [2, 3], high-resolution earth observation systems [4, 5], and lithography machines [5]. However, their diameter and accuracy restrict the performance of related equipment. For example, the primary mirrors of the Thirty Meter Telescope [6] and the 42-m European Extremely Large Telescope (E-ELT) [2] consist of 492 and 798 quasi-hexagonal mirror segments, respectively, with a diagonal length of 1.45 m. The National Ignition Facility [1] in the USA and the Megajoule Laser [7] in France require 7360 and 4200 large-aperture optical elements, respectively. The typical manufacturing process of aspheric optics comprises grinding [8], polishing [9, 10], and focused ion beam figuring [11]. The material removal rates of the polishing and figuring processes are extremely low. Therefore, the form error and subsurface damage depth [12] induced by the grinding process should be reduced to minimize the required material removal depth in the subsequent processes.

Hence, considerable technological advancements pertaining to ultra-precision grinding of large-aperture mirrors have been achieved. The Steward Laboratory at the University of Arizona developed the large optical generator to grind and polish 8 m mirrors [13]. It was successfully used to machine the 6.5-m primary mirror of the Magellan telescope [14] and 8.4-m primary mirrors of the Large Binocular Telescope [14, 15]. The form error of these mirrors can be reduced to less than 10 μm RMS after grinding. Researchers at the Cranfield University developed a large ultra-precision grinding machine,

*Correspondence: sunlin@xjtu.edu.cn

[1] State Key Laboratory for Manufacturing Systems Engineering, Xi'an Jiaotong University, Xi'an 710049, China
Full list of author information is available at the end of the article

OAGM2500 [16–18], for the manufacturing of large mirrors used in telescopes. Its maximum machinable aperture and achievable relative form error are Φ2500 mm and $1/10^6$ PV, respectively. Subsequently, another large ultra-precision grinding machine, Big OptiX [17, 18], was developed to achieve high-efficiency and low-damage grinding of hard and brittle materials. By employing a novel *R*-theta grinding mode with an inclined toroidal shape diamond wheel, a high material removal rate of 187.5 mm^3/s was achieved when grinding the 1.45-m Zerodur mirror [18] used for the E-ELT telescope. The form error and subsurface damage depth were reduced to less than 1 μm RMS and 8 μm, respectively, within a manufacturing cycle of < 20 h. The ULTRASONIC100-5 machining center developed by DMG MORI Company Ltd. integrates ultrasonic vibration with traditional grinding to improve the machining efficiency of hard and brittle materials. Using this machine, the form error of a 700 mm × 700 mm SiC high-order off-axis aspheric mirror was efficiently reduced to 2.13 μm RMS [19]. Other companies, such as Blohm, Satisloh, Schneider, and Optotech, provide large aspheric grinding machines with a machinable diameter of Φ500–2000 mm.

China has conducted comprehensive studies pertaining to the ultra-precision grinding of large-aperture optics in recent years. For example, researchers at Tsinghua University developed a six-axis, large-scale precision grinding machine. Grinding tests of a Φ770 mm K9 glass show that the form error was less than 10 μm, and the surface roughness can reach the submicron level. The AOCMT ultra-precision grinding machine [20] developed by the National University of Defense Technology can machine optical elements up to a diameter of 650 mm. It has been successfully used to grind a Φ116 mm parabolic SiC workpiece to a form error of 8.9 μm. The Changchun Institute of Optics and Fine Mechanics developed a series of four-axis aspheric machine tools, namely, the 800-mm FSGJ-1 [21], 1.2-m FSGJ-2 [22], and 2-m FSGJ-3. These machines integrated the functions of rough grinding, fine grinding, polishing, and online measurement. Using the computer-controlled optical surfacing technique, a form precision of 12 nm RMS for a 1-m mirrors was achieved. In recent years, Jiang et al. at Xi'an Jiaotong University developed two ultra-precision aspheric grinding machines with maximum machinable diameters of Φ900 mm [23, 24] and Φ1500 mm [25, 26]. The achievable form error for a 400-mm mirror was smaller than 5 μm PV using the arc envelope grinding method.

The studies above indicate that it is challenging to efficiently achieve an extremely high form accuracy by grinding, e.g., 5 μm/m PV, for large aspheric optics. During the grinding of such optics, the tool setting error is one of the main error sources of the workpiece form error. For a specified geometry of the machined surface, the grinding path is determined by the geometry of the grinding wheel and the spatial locations of the wheel and workpiece. Therefore, the tool position in the *X*-, *Y*-, and *Z*-directions must be adjusted during the grinding process. The tool setting in the *X*- and *Y*-directions ensures the lowest point of the grinding wheel coincides with the axis of the turntable. The tool setting in the *Z*-direction determines the height of the grinding wheel relative to the workpiece.

The outer cylindrical surface and upper plane of the workpiece can be used as reference surfaces during the rough setting of the wheel. When the wheel is set in the *X*-direction, it approaches the outer cylindrical surface from both the positive and negative directions of the *X*-axis. The *X*-coordinates of the machine tool in the contact state are recorded as x_1 and x_2. The middle point between x_1 and x_2, i.e., $x_0 = (x_1 + x_2)/2$, is the zero point of the workpiece in the *X*-direction. However, the accuracy of the wheel setting method mentioned above is limited by the form error of the cylindrical surface. In addition, the contact state between the wheel and workpiece is difficult to be determined accurately. Therefore, other methods should be developed by clarifying the evolution of the workpiece form error with the wheel setting errors.

The tool setting problem has been intensively investigated [27, 28] to improve machining precision. Typical contact-type tool setting methods include on-machine touch probes [28] and force sensors [29, 30], whereas examples of non-contact methods include acoustic emission sensors [31], digital microscopes [32], and digital holography [33]. However, studies pertaining to wheel setting for the grinding of aspheric optics are rare. Chen et al. [34] discovered that inward and outward offsets generated V-shaped and Λ-shaped profiles, respectively. However, the relationship between wheel setting error and workpiece form error has not been analytically modeled. Kang et al. [35] modeled and analyzed the form error of aspheric surfaces subjected to grinding with a cup wheel. The key error sources were discovered to be the tool setting error and radius error of the grinding wheel. Nevertheless, elaborate numerical computations were required to obtain the form error. Wei et al. [26] and Xi et al. [24] developed analytical tool setting error models that encompassed both the radial and lateral directions. However, these models did not account for the variation in the grinding point during arc envelope grinding; as such, the prediction accuracy was limited, especially for steep aspheric surfaces.

To overcome these challenges, the relationship between the form error of aspheric optics and the setting error of an arc grinding wheel was modeled

analytically and numerically by considering the variation in the grinding point on the wheel. A grinding example is presented herein to verify the form error model and a newly proposed compensation method.

2 Modeling of Aspherical Surface Generation

2.1 Geometric Representation of Aspherical Surface

An aspheric surface is a rotationally symmetrical surface that deviates from a spherical surface in shape. A spherical or aspherical surface with a vertex at the origin and an optical axis along the Z-axis can be expressed as

$$z(h) = \frac{ch^2}{1+\sqrt{1-(1+k)c^2h^2}} + \sum A_m h^{2m}, \quad (1)$$

where $c = 1/R_0$ is the vertex curvature; R_0 is the vertex curvature radius; h is the radial distance from the optical axis (Figure 1); k is the conic constant that determines the shape of the surface; $A_m h^{2m}$ represents the high-order terms of the aspherical surface, where m is an integer.

Eq. (1) is reduced to a quadratic aspheric surface if higher-order terms are absent. It can be rewritten as

$$\frac{\left(z-\frac{1}{(1+k)c}\right)^2}{\left(\frac{1}{(1+k)c}\right)^2} + \frac{h^2}{\left(\frac{1}{\sqrt{1+k}c}\right)^2} = 1. \quad (2)$$

For a point P (x, y, z) on a quadratic aspherical surface Figure 2), its coordinates can be expressed as a parametric equation, i.e.,

$$\begin{cases} x = h\cos\theta, \\ y = h\sin\theta, \\ z = \frac{ch^2}{1+\sqrt{1-(1+k)c^2h^2}}, \end{cases} \quad (3)$$

where θ is the angle between the positive direction of the X-axis and the projected vector of $\overrightarrow{OP}$ on the XOY plane, as shown in Figure 2.

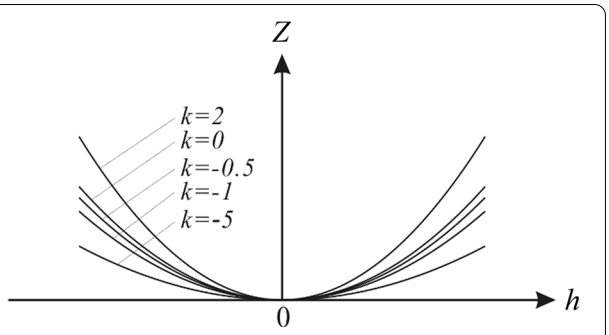

Figure 1 Surfaces corresponding to different conic constants k

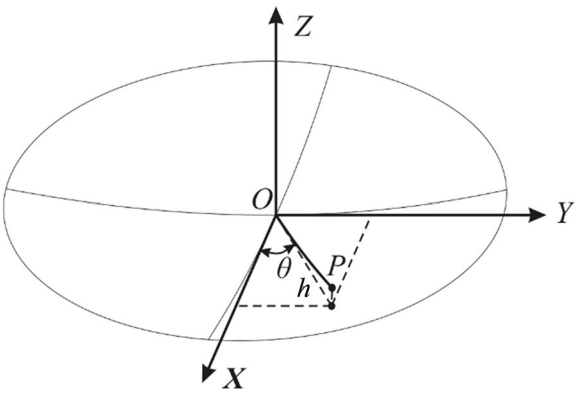

Figure 2 Coordinate system of aspheric workpiece

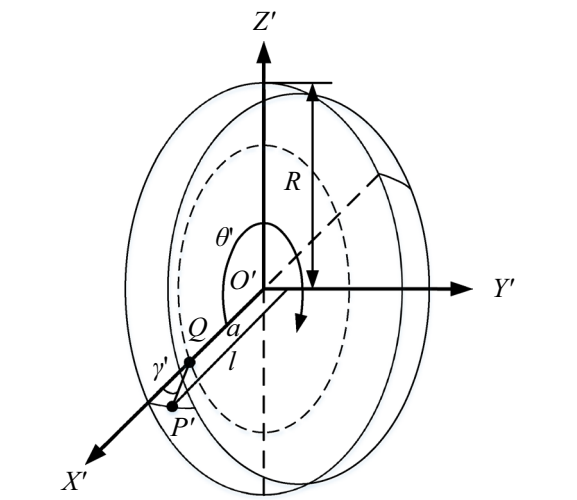

Figure 3 Coordinate system of grinding wheel (Only region of $Y' \geq 0$ is shown, since wheel is symmetrical about $X'O'Z'$-plane)

2.2 Geometric Representation of Arc Grinding Wheel

A parallel grinding wheel with a circular arc was used for the arc envelope grinding of aspheric optical elements. The coordinate system of the grinding wheel is illustrated in Figure 3. The Y'-axis was along the wheel axis, and the origin O' was located at the intersection of the Y'-axis and the axial symmetrical surface of the wheel. The wheel radius in this symmetry plane, i.e., $X'O'Z'$ coordinate plane, was R. The wheel surface with abrasive grains was rotationally symmetrical along the Y'-axis. Its generatrix is an arc with a radius $QP' = r$. The distance from the arc center Q to the wheel axis is $a = R - r$. The distance from point P' on the wheel surface to the Y'-axis is denoted as l. The angle between the line $P'O'$ and $X'O'Y'$ plane is θ' (clockwise), which ranges from 0° to 360°. The angle between the radius QP' and the $X'O'Z'$ plane is γ'.

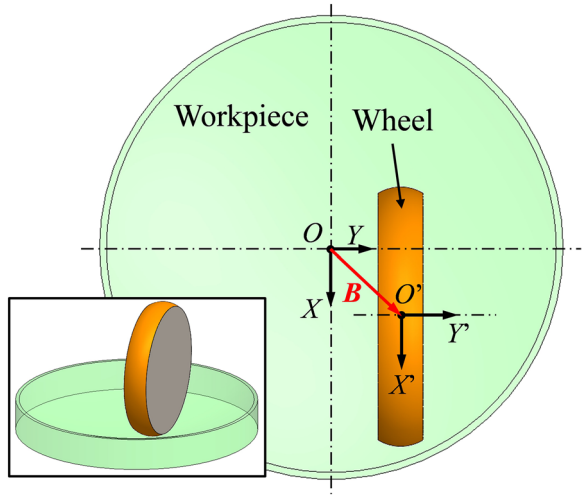

Figure 4 Coordinate systems for grinding of aspheric surface using arc wheel

In the $O'X'Y'Z'$ coordinate system, the wheel surface can be described by the following equations:

$$\begin{cases} x' = l\cos\theta', \\ y' = r\sin\gamma', \\ z' = l\sin\theta', \\ l = a + r\cos\gamma', \end{cases} \tag{4}$$

where the range of γ' is $-\arcsin\left(W/2r\right) \le \gamma' \le \arcsin\left(W/2r\right)$, where W is the width of the grinding wheel.

2.3 Modeling of Aspherical Surface Generation

During the modeling of the generation process of the aspherical surface, the X-, Y-, and Z-axes of the workpiece coordinate system are assumed to be parallel to the X'-, Y'-, and Z'-axes of the wheel coordinate system, respectively, as shown in Figure 4. The workpiece surface was tangential to the wheel surface during grinding at the grinding point. The positions of the grinding point on both the wheel and workpiece changed during grinding. The coordinates in the wheel coordinate system can be transformed into the workpiece coordinate system via the following translation transformation:

$$\begin{bmatrix} x \\ y \\ z \end{bmatrix} = \begin{bmatrix} x' \\ y' \\ z' \end{bmatrix} + \boldsymbol{B}, \tag{5}$$

where $\boldsymbol{B} = \overrightarrow{OO'}$ is the translation vector, which corresponds to the coordinates of O' in the workpiece coordinate system. O' is the programming point and its trajectory is the grinding path.

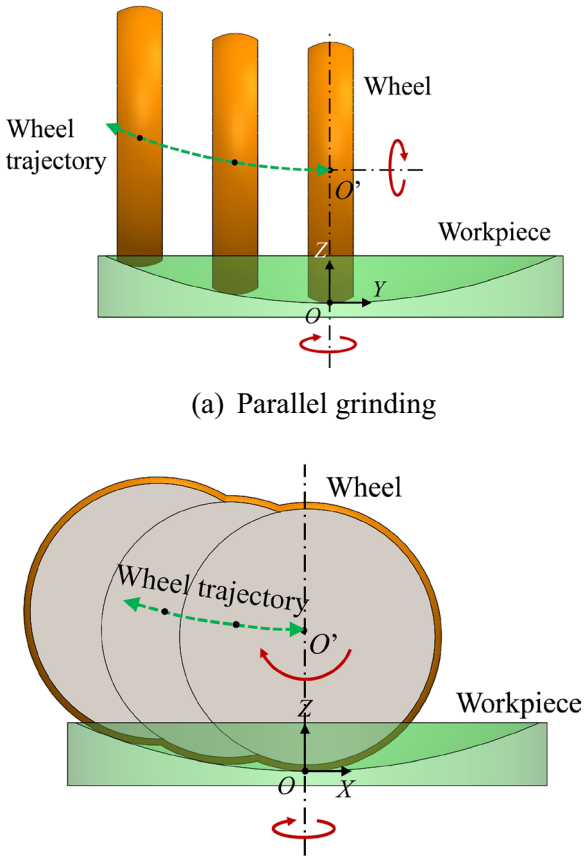

Figure 5 Parallel grinding and cross grinding of aspherical surfaces using arc grinding wheel

$$\boldsymbol{B} = \begin{bmatrix} X_s \\ Y_s \\ Z_s \end{bmatrix}. \tag{6}$$

In the initial grinding state, the X- and Y-components of $\boldsymbol{B}_0$ represent the wheel setting errors along the tangential and axial directions of the wheel, respectively.

For parallel grinding, the wheel moves along the Y- and Z-axes, and the velocity directions of the grinding wheel and workpiece are parallel at the grinding point, as shown in Figure 5a. Therefore, X_s in vector $\boldsymbol{B}$ remains constant and is the lateral wheel setting error. For cross grinding, the wheel moves along the X- and Z-axes, and the velocity directions of the wheel and workpiece are perpendicular to each other at the grinding point, as shown in Figure 5b. Hence, Y_s remains constant during grinding and is the lateral wheel setting error.

The grinding point is the intersection point between the workpiece and wheel surfaces. Combining Eqs. (3)–(5) yields

$$\begin{bmatrix} h\cos\theta \\ h\sin\theta \\ \frac{ch^2}{1+\sqrt{1-(1+k)c^2h^2}} \end{bmatrix} = \begin{bmatrix} (a+r\cos\gamma')\cos\theta' \\ r\sin\gamma' \\ (a+r\cos\gamma')\sin\theta' \end{bmatrix} + \begin{bmatrix} X_s \\ Y_s \\ Z_s \end{bmatrix}. \tag{7}$$

In addition, the workpiece surface is tangential to the wheel surface at the grinding point. Therefore, the normals of the workpiece and wheel surfaces are collinear at the grinding point. The normal vector at point $P(h, \theta)$ on the aspherical surface can be expressed as

$$\vec{n}_s = \begin{bmatrix} \frac{\partial(y,z)}{\partial(h,\theta)} \\ \frac{\partial(z,x)}{\partial(h,\theta)} \\ \frac{\partial(x,y)}{\partial(h,\theta)} \end{bmatrix} = \begin{bmatrix} -\frac{\mathrm{d}z}{\mathrm{d}h}h\cos\theta \\ -\frac{\mathrm{d}z}{\mathrm{d}h}h\sin\theta \\ h \end{bmatrix}, \tag{8}$$

where

$$\frac{\mathrm{d}z}{\mathrm{d}h} = z'(h) = \frac{ch}{1+\sqrt{1-(k+1)c^2h^2}} \left(2+\frac{(k+1)c^2h^2}{\left(1+\sqrt{1-(k+1)c^2h^2}\right)\sqrt{1-(k+1)c^2h^2}}\right). \tag{9}$$

Similarly, the normal vector at point $P'(\gamma', \theta')$ on the grinding wheel can be written as

$$\vec{n}_w = \begin{bmatrix} \frac{\partial(y,z)}{\partial(\gamma',\theta')} \\ \frac{\partial(z,x)}{\partial(\gamma',\theta')} \\ \frac{\partial(x,y)}{\partial(\gamma',\theta')} \end{bmatrix} = \begin{bmatrix} r\left(a+r\cos\gamma'\right)\cos\gamma'\cos\theta' \\ r\left(a+r\cos\gamma'\right)\sin\gamma' \\ r\left(a+r\cos\gamma'\right)\sin\theta'\cos\gamma' \end{bmatrix}. \tag{10}$$

The normals of the workpiece and wheel surfaces at the grinding point are collinear. Therefore, the following equations can be obtained:

$$\frac{-\frac{\mathrm{d}z}{\mathrm{d}h}h\cos\theta}{r(a+r\cos\gamma')\cos\gamma'\cos\theta'} = \frac{-\frac{\mathrm{d}z}{\mathrm{d}h}h\sin\theta}{r(a+r\cos\gamma')\sin\gamma'} = \frac{h}{r(a+r\cos\gamma')\sin\theta'\cos\gamma'}. \tag{11}$$

The coordinates of the grinding point can be obtained by solving Eqs. (7) and (11). Subsequently, the corresponding grinding path $Z_s = f(X_s)$ or $Z_s = f(Y_s)$ can be obtained as follows:

$$\begin{bmatrix} h\cos\theta \\ h\sin\theta \\ z(h) \end{bmatrix} = \begin{bmatrix} (a+r\cos\gamma')\cos\theta' \\ r\sin\gamma' \\ (a+r\cos\gamma')\sin\theta' \end{bmatrix} + \begin{bmatrix} X_s \\ Y_s \\ Z_s \end{bmatrix}. \tag{12}$$

If the grinding path is known, then the expression of $z(h)$ can be obtained by solving Eqs. (11) and (12).

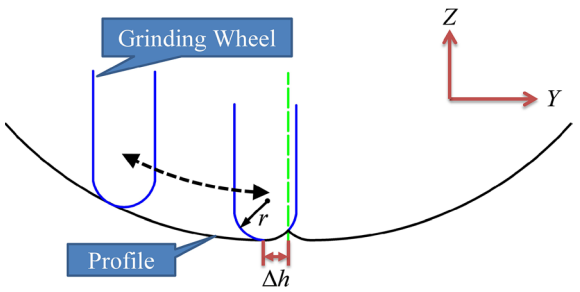

(a) Schematic diagram

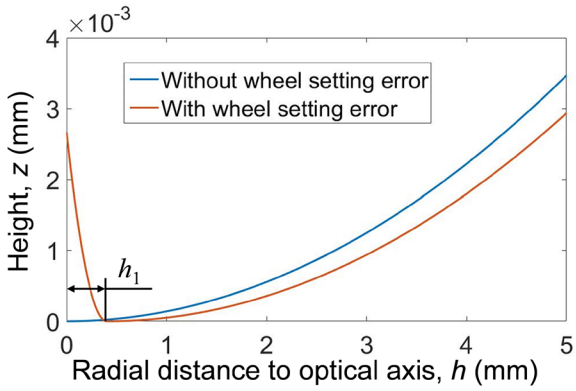

(b) Simulation results

Figure 6 Effect of wheel setting error along outward feed direction on workpiece profile during parallel grinding ($\Delta h = 0.4$ mm)

3 Effect of Wheel Setting Error on Workpiece Form Error

The effect of the wheel setting error on the workpiece geometry can be clarified using the generation model of aspherical surface established above. The aspheric surface is a long ellipsoid with $c = 1/3600$ and $k = -0.2$. The wheel is an arc-shaped parallel wheel with $R = 175$ mm and $r = 30$ mm. This r value renders the wheel suitable for grinding aspheric surfaces with vertex curvature radii ranging from hundreds to thousands of millimeters. It is assumed that the grinding wheel moves from the center of the workpiece to the outside during grinding.

3.1 Wheel Setting Error in Feed Direction

If the wheel setting error is in the outward feed direction (Figure 6a), then the resultant surface profile of the workpiece can be expressed by the following piecewise function:

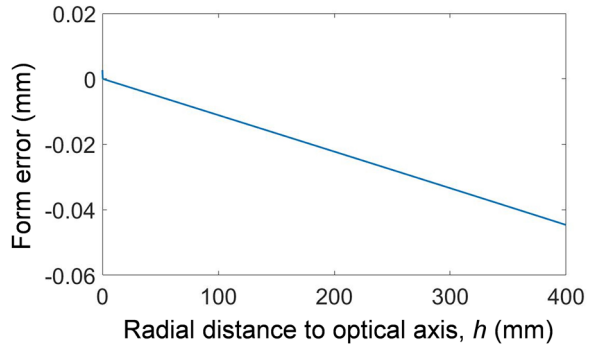

Figure 7 Evolution of workpiece form error with radial distance to optical axis for $\Delta h = 0.4$ mm

$$z_1(h) = \begin{cases} \frac{c(h-\Delta h)^2}{1+\sqrt{1-(k+1)c^2(h-\Delta h)^2}}, & h \geq h_1, \\ \frac{c_s(h-\Delta h)^2}{1+\sqrt{1-c_s^2(h-\Delta h)^2}}, & h < h_1, \end{cases} \tag{13}$$

where Δh is the wheel setting error along the feed direction. The value of h_1 can be determined by the continuity of the piecewise function; $h_1 \approx \Delta h$ if $\Delta h \ll 1/c_s$. Figure 6a indicates that the surface profile is a circular arc in the region $h \leq h_1$. The radius of this arc is equal to r and R for parallel and cross grinding, respectively. c_s in Eq. (13) refers to the vertex curvature. If parallel and cross grinding are performed using an arc-shaped parallel wheel, then $c_s = 1/r$ and $1/R$, respectively. Eq. (13) indicates that the form error in the circular arc segment will be less sensitive to the wheel setting error if a larger radius of the wheel arc profile is used. Compared with parallel grinding, the form error for cross grinding is more sensitive to the wheel setting error in these segments because $r < R$.

Figure 6b compares the workpiece profiles with and without wheel setting error. When the setting error was along the outward feed direction, the workpiece profile was composed of a circular arc and an elliptic curve. As shown in Figure 7, the workpiece form error was negative and decreased linearly with h in the region $h \geq h_1$. The form error at 400 mm induced by a wheel setting error of 0.4 mm was -0.0446 mm during parallel grinding.

For the inward tool setting error (Figure 8a), the surface profile of the workpiece after parallel grinding can be expressed by the following piecewise function:

$$z_1(h) = \begin{cases} \frac{c(-h-\Delta h)^2}{1+\sqrt{1-(k+1)c^2(-h-\Delta h)^2}}, & h < h_2, \\ \frac{c_s(-h-\Delta h)^2}{1+\sqrt{1-c_s^2(-h-\Delta h)^2}}, & h_2 \leq h < h_3, \\ \frac{c(h-\Delta h)^2}{1+\sqrt{1-(k+1)c^2(h-\Delta h)^2}}, & h \geq h_3. \end{cases} \tag{14}$$

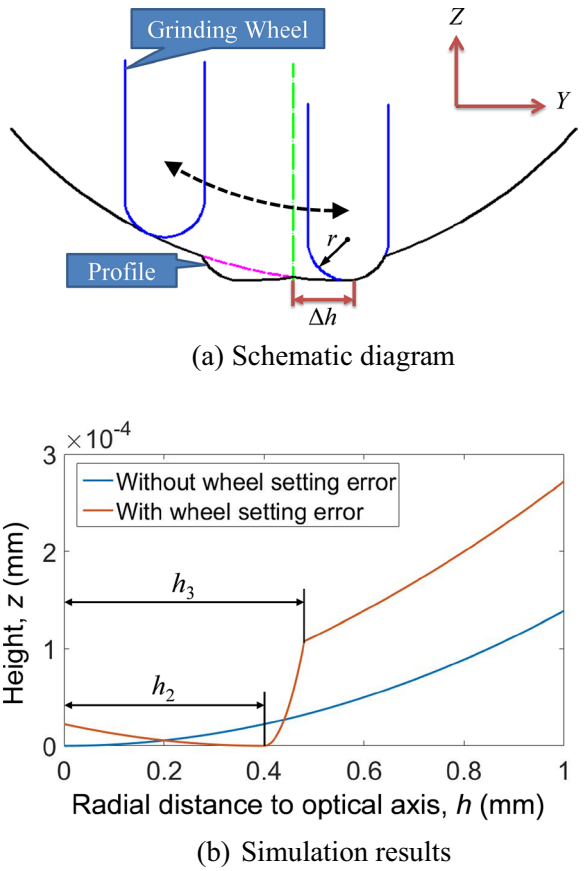

Figure 8 Effect of inward wheel setting error on workpiece profile during parallel grinding ($\Delta h = -0.4$ mm)

The values of c_s, c, and k are known for a specified wheel and aspheric surface. Therefore, the values of h_2 and h_3 can be determined using the continuity condition of the curve; $h_2 \approx \Delta h$ if $\Delta h \ll 1/c_s$. The profile of the workpiece is composed of two elliptic curves and one circular arc, as shown in Figure 8. Figure 9 shows that the form error increased linearly with h in the region $h \geq h_3$. A tool setting error Δh of -0.4 mm resulted in a form error of 0.0447 mm at a radius of 400 mm. Its absolute value was extremely close to that induced by $\Delta h = 0.4$ mm. Therefore, the direction and magnitude of the wheel setting error determined the shape and magnitude of the form error profile, respectively.

The wheel setting error determines the slope between the form error and h. Simulations (see Figure 10) show that the absolute value of the slope increased linearly with the wheel setting error in the feed direction. This relationship can be used to determine the value of the wheel setting error.

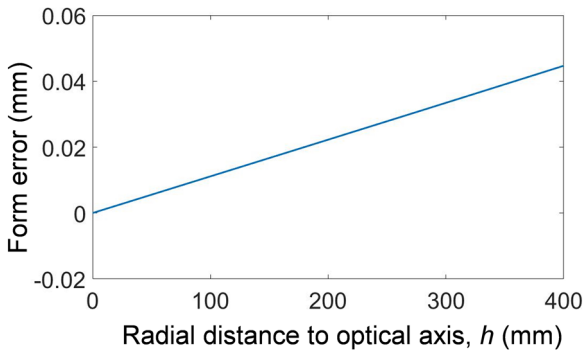

Figure 9 Evolution of workpiece form error with radial distance to optical axis during parallel grinding ($\Delta h = -0.4$ mm)

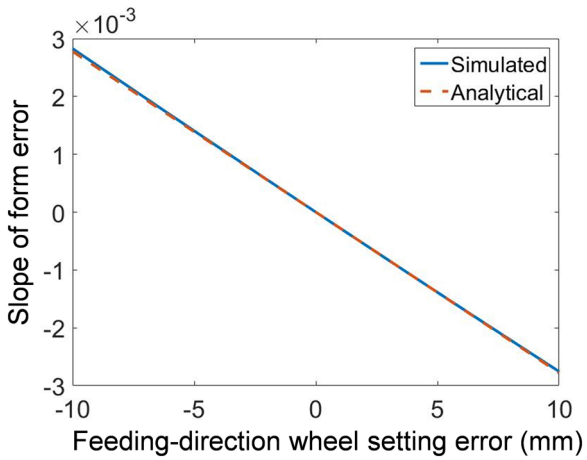

Figure 10 Slope of workpiece form error as a function of wheel setting error in feed direction

The relationship between the slope of the form error and the wheel setting error can be obtained via theoretical analysis. When Δh is small, the form error in the region $h \geq h_1$ (or $h \geq h_3$) can be expressed via the Taylor expansion, as follows:

$$e_z = z_1(h) - z(h) \approx -z'(h)\Delta h, \tag{15}$$

where z_1 and z are the actual and ideal profiles, respectively. e_z for a quadratic aspheric surface is expressed as

$$e_z \approx -\frac{ch}{1+\sqrt{1-(k+1)c^2h^2}} \left(2+\frac{(k+1)c^2h^2}{\left(1+\sqrt{1-(k+1)c^2h^2}\right)\sqrt{1-(k+1)c^2h^2}}\right)\Delta h. \tag{16}$$

$h \ll R_0$ and $(k+1)c^2h^2 \ll 1$ because $h \leq 400$ mm and $R_0 = 3600$ mm in this study. Eq. (16) can be reduced to $e_z \approx -ch\Delta h$. Therefore, the form error is a bilinear function of h and Δh. This is consistent with the simulation results shown in Figures 7, 8, 9, 10. The value of e_z can be calculated using Eqs. (13) or (14) when $h \ll R_0$ is not satisfied.

3.2 Lateral Wheel Setting Error

The form error of the workpiece in the region $h \geq \Delta l$ caused by the lateral wheel setting error Δl can only be solved using numerical methods. X_s equals Δl for parallel grinding, whereas Y_s and Z_s follow the trajectory without the wheel setting error. For cross grinding, Y_s is equal to Δl, whereas X_s and Z_s follow the trajectory without the wheel setting error. Subsequently, the surface profile and form error of the workpiece in the region $h \geq \Delta l$ can be obtained by numerically solving Eqs. (11) and (12).

The surface profile of the workpiece in the region $h < \Delta l$ is a circular arc expressed as follows:

$$z_1(h) = \frac{c_s(h-\Delta l)^2}{1+\sqrt{1-c_s^2(h-\Delta l)^2}}. \tag{17}$$

For parallel and cross grinding using arc grinding wheels, c_s is equal to $1/R$ and $1/r$, respectively.

The effects of the lateral wheel setting error on the surface profile and its form error are shown in Figure 11. The maximum form error was recorded at the center of the aspherical surface. It is smaller than 0.1 μm because c_s was extremely small in this study. The form error remained almost constant in the region $h \geq \Delta l$, with a slight decrease as h increased.

Because the c_s value for cross grinding was much greater than that for parallel grinding, the maximum form error for cross grinding was much greater than that for parallel grinding, as indicated by Figures 11 and 12. The form error of the workpiece in the region $h \geq \Delta l$ was extremely small and almost constant, which is similar to parallel grinding. It is noteworthy that the abrupt change shown in Figure 12b might be induced by the error in the numerical calculation, since the form error in this region was as low as 2.24×10^{-5} mm.

In summary, the form error was more sensitive to the feed-direction wheel setting error than the lateral wheel setting error during the grinding of large-aperture aspherical surfaces. The maximum form error induced by the feed-direction wheel setting error was recorded at the rim of the workpiece. It exhibited a bilinear relationship with the wheel setting error and the distance to the optical axis. By contrast, the maximum form error of the workpiece caused by the lateral wheel setting error was recorded at the center of the workpiece. The form error in the central region was more sensitive to the wheel

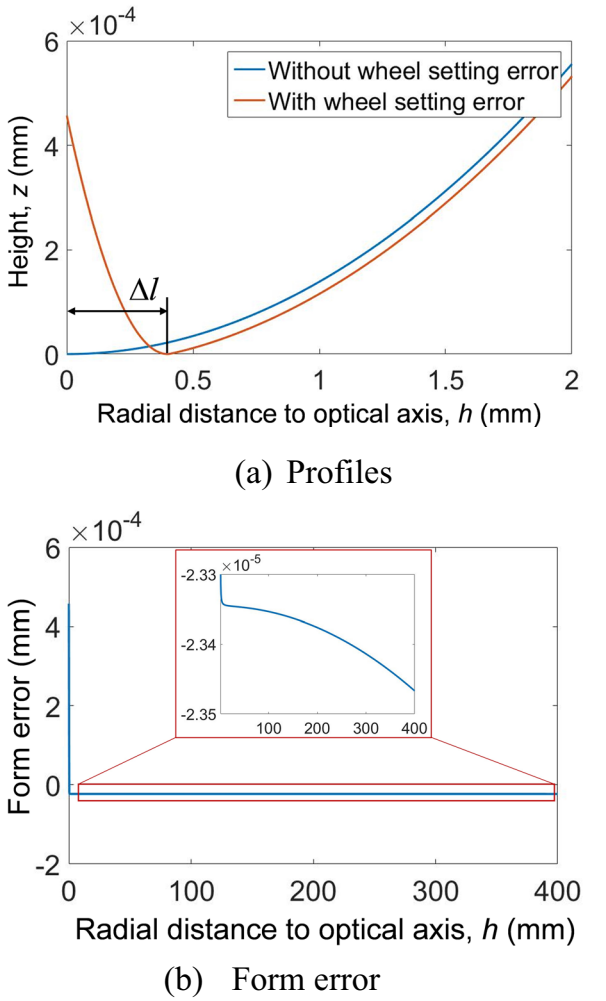

Figure 11 Effect of lateral wheel setting error on workpiece profile for parallel grinding (Δl=0.4 mm)

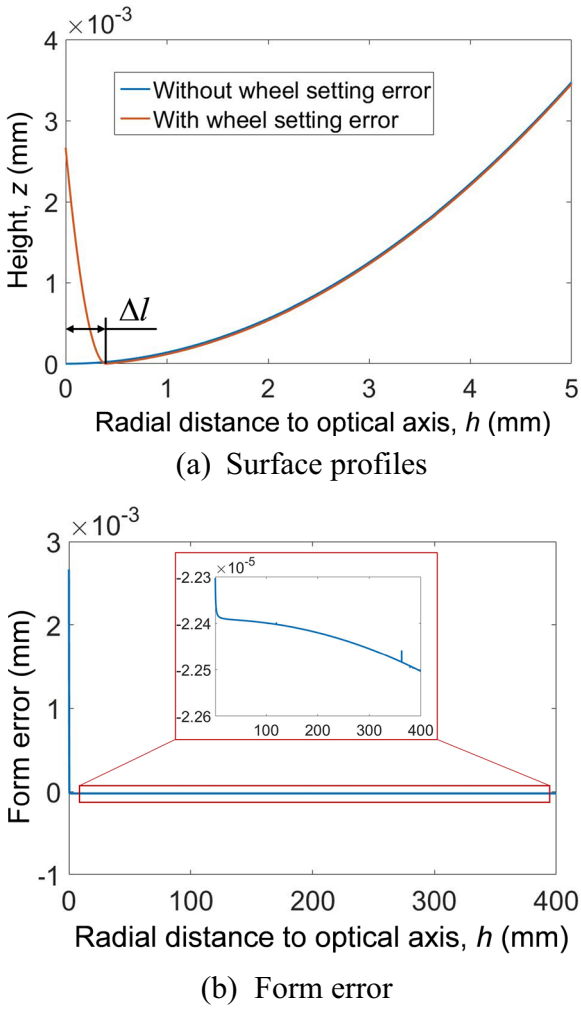

Figure 12 Workpiece profiles and form error as a function of h for cross grinding with lateral wheel setting error of Δl=0.4 mm

setting error in the axial direction of the grinding wheel than that in the tangential direction.

4 Error Compensation and Grinding Tests

4.1 Error Compensation

Because the form error was insensitive to the wheel setting error along the lateral direction, only the feed-direction wheel setting error was considered during the grinding of the large-aperture aspheric surfaces. After determining the slope between the form error and h via measurement, the value of the wheel setting error Δh was calculated using Eq. (16).

The dashed line in Figure 13 represents the measured error curve of the workpiece after the wheel changing process. It comprises two straight lines forming the V shape, which is consistent with the theoretical error curve induced by the wheel setting error Δh = 2.89 mm,

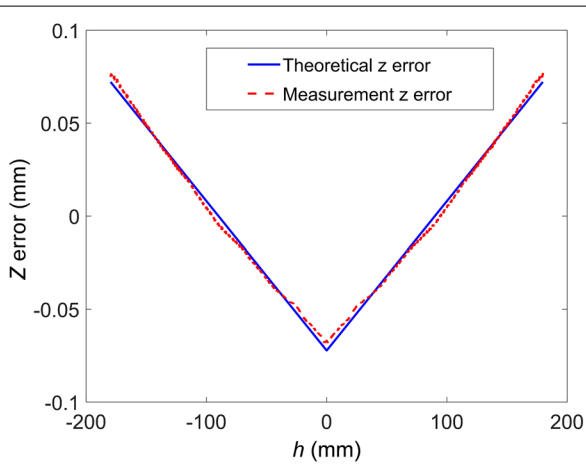

Figure 13 Theoretical and measured error curves caused by wheel setting error

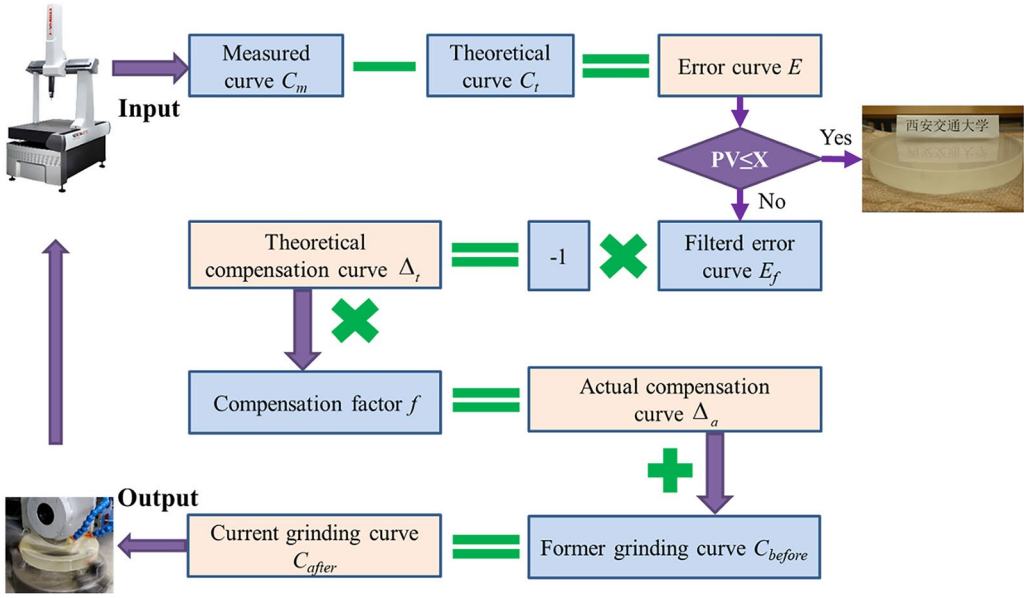

Figure 14 Error compensation during grinding

i.e., the solid line in Figure 13. This indicates that inappropriate wheel changing process results in a significant wheel setting error. The wheel setting error determined by the above method was used for wheel adjustment during the subsequent grinding process.

In this study, off-line measurement was adopted during the fine grinding stage. Hence, repetitive workpiece clamping was required within the compensation cycles. Figure 13 and Ref. [24] indicate that wheel setting errors of 2.89 mm and 0.866 mm occurred during the grinding of large-aperture aspherical optics, respectively. Figure 6 and Figure 8 indicate that a tool setting error of 0.4 mm resulted in a form error of 0.0447 mm at a radius of 400 mm. Therefore, it is essential to accurately adjust the wheel position during the grinding of large-aperture aspherical optics.

After adjusting the wheel to the correct position, the error compensation method shown in Figure 14 was used to further reduce the machining error. First, a coordinate measuring machine (CMM) (Leitz Reference HP, Hexagon, China) was used to measure the profile of the aspherical generatrix, and the error curve E was obtained by subtracting the theoretical curve from it. Subsequently, the low-pass filtering of E was performed to eliminate the effects of random machining errors, which resulted in a filtered error curve E_f. The theoretical compensation curve Δ_t was the opposite number of E_f. A compensation factor f was introduced to obtain the actual compensation curve Δ_a. Finally, the current grinding curve C_{after} was obtained by summing up Δ_a and the former grinding curve C_{before} (i.e., the envelope of the outer circumference of the grinding wheel).

The original grinding path was obtained using the method described in Section 2.3, and the errors of the machine tool, wheel wear, and wheel setting were not considered. During the error compensation stage, the trajectory of the wheel center, i.e., the grinding path $Z_s = f(X_s)$ or $Z_s = f(Y_s)$, was obtained by solving Eqs. (7) and (11) using C_{after} as the input. Subsequently, the grinding path was used to machine the workpiece. If the PV value of the form error measured by the CMM was out of the tolerance, then a compensation grinding process was performed based on the measured error curve until the form error satisfied the requirement.

The tilt of the error curve was adjusted before calculating the form error to eliminate the effect of the workpiece clamping error. The equation for the symmetry axis of the aspherical surface was assumed to be $z = kx + b$. The slope k and intercept b were varied at certain intervals to determine their optimal values. For each k and b value, the measurement points $P_l(h_1, z_1)$ on the left side of the symmetry axis were mirrored to the right side to obtain the mirror points $P'_l(h'_1, z'_1)$. The measurement points $P_r(h_2, z_2)$ on the right side of the symmetry axis were interpolated to obtain the interpolation points $P'_r(h'_1, z'_2)$. Subsequently, the Z-direction difference $e_z(h'_1)$ between each mirror point and its corresponding interpolation point was calculated. The k and b values resulting in the smallest root mean square of $e_z(h'_1)$ defined the optimal symmetry axis. Finally, the

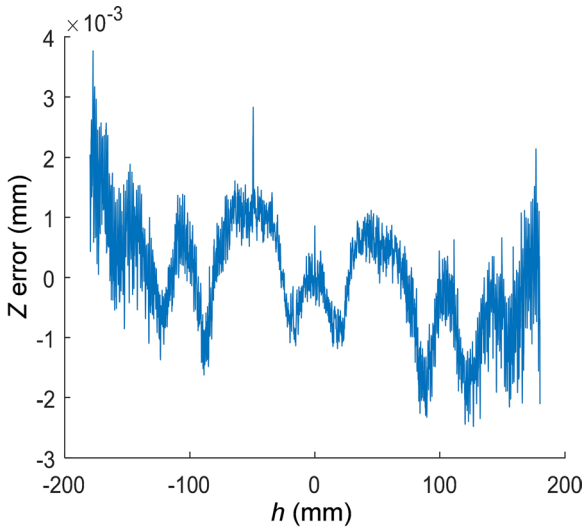

(a) Before correction

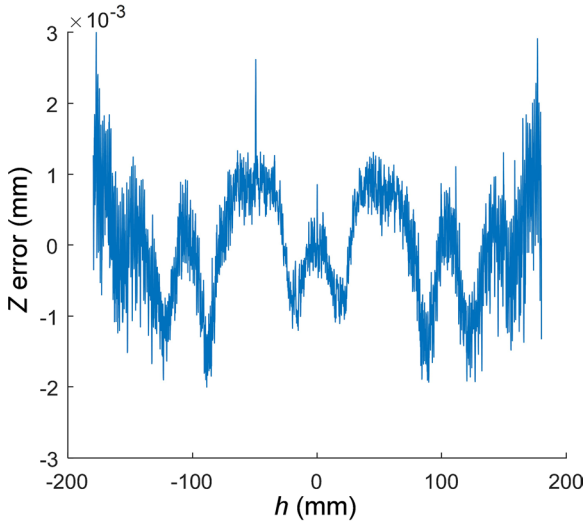

(b) After correction

Figure 15 Error curves of workpiece generatrix before and after tilt correction

error curve was rotated to achieve a vertical symmetry axis. The error curves before and after tilt correction are shown in Figure 15a and b, respectively.

The optimal compensation factor depends on the ratio of the actual material removal depth to the nominal grinding depth; it is governed by the machine stiffness, machine precision, and process parameters. Currently, it is difficult to theoretically model the quantitative relationship between the nominal grinding depth and actual material removal depth. Therefore, the compensation factor was determined via grinding tests in this study.

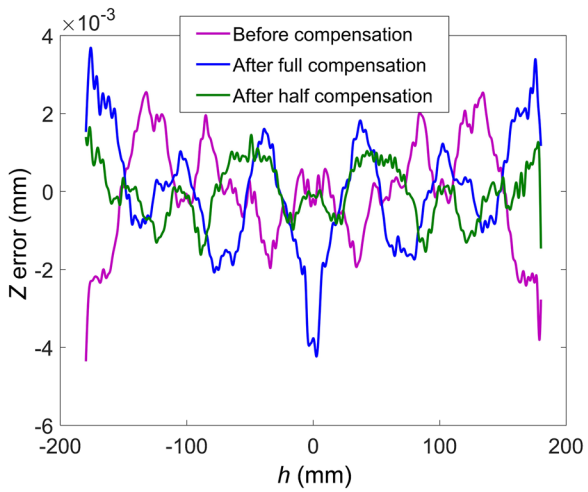

Figure 16 Error curves of workpiece generatrix before and after compensation

An error compensation factor of 1:1 was appropriate for rough grinding. However, it was discovered that a compensation factor of 1:1 resulted in overcompensation in the fine grinding stage, as revealed by Figure 16. Consequently, the locations of the peaks before compensation corresponded well to the valleys after compensation. The form error of 6.9 μm PV after compensation was similar to that before compensation, i.e., 7.9 μm PV. Therefore, a compensation factor of 0.5 was adopted in the fine grinding stage. The form error was reduced significantly to 3.3 μm PV after grinding using the abovementioned factor.

4.2 Grinding Tests

Parallel grinding tests of K9 glass with a diameter of Φ400 mm were performed on a large grinding machine (CM1500, Xi'an Jiaotong University, China), as shown in Figure 17. The maximum machinable diameter of the machine tool is ≥ Φ1500 mm. The strokes of the *X*- and *Z*-axes were 1800 and 400 mm, respectively. Linear encoders (LC183, HEIDENHAIN, Germany) with a resolution of 10 nm were used in all three linear axes to provide a high positioning resolution. A high-stiffness hydrostatic spindle with a runout of ≤ 0.2 μm was used to achieve high machining precision. The geometries of the workpiece and grinding wheel were consistent with those used in the simulation. The grinding process comprised three stages: rough grinding, semi-finishing grinding, and fine grinding.

The process parameters for all the grinding stages are listed in Table 1. A D151 metal-bonded diamond grinding wheel with a grain dimension of 127–160 μm was used in the rough grinding stage to ensure a high material

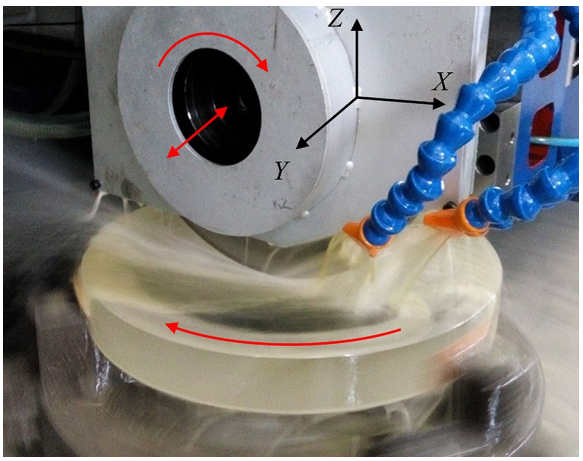

Figure 17 Grinding of Φ400 mm K9 glass blank on CM1500 large grinding machine

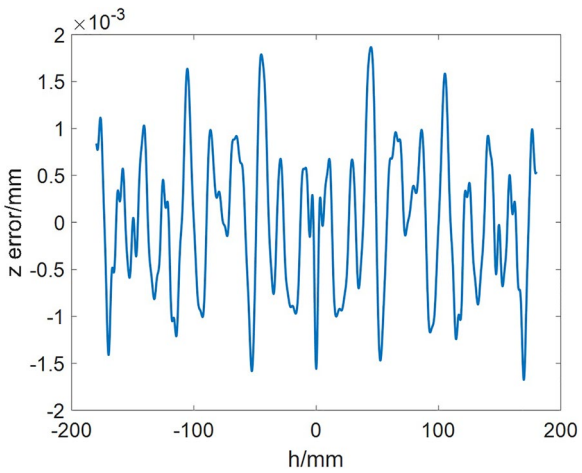

Figure 18 Error curve of aspherical surface after grinding. Surface roughness was removed using a low-pass filter

Table 1 Process parameters

Grinding stage	Grit designation	Wheel speed (r/min)	Workpiece speed (r/min)	Grinding depth (mm)	Feed rate (mm/min)
Rough	D151	2000	10	0.5	10–30
Semi-finish	D46	2300	15	0.05–0.1	10–20
Fine	D15A	2500	15	0.005	2–5

removal rate. A D46 metal-bonded diamond wheel with a grain dimension of 40–50 μm was used in the semi-finishing stage. A shallower grinding depth and a lower feed rate were adopted in this stage to reduce the form error to less than 5 μm. A D15A resin-bonded diamond wheel with a grain dimension of 10–15 μm was used in the fine grinding stage to reduce the surface roughness and subsurface damage depth. A cup truer provided by Guo et al. was used to dress the arc-profile diamond wheels. The dressing principle and conditions are described in Refs. [36, 37]. A form error of 3.4 μm PV was achieved after error compensation using the process parameters listed in Table 1, as shown in Figure 18.

5 Conclusions

In this study, analytical and numerical form error models of aspherical optical elements induced by wheel setting errors were established for both parallel and cross grinding. The effects of the direction of the wheel setting error on the shape and sensitivity of the form error were analyzed. The main conclusions are as follows.

(1) The expressions of workpiece profiles induced by the wheel setting error were piecewise functions in most cases. Their forms were independent of the grinding mode. However, compared with parallel grinding, the ground form error for cross grinding was more sensitive to the wheel setting error in the circular arc segments of the profiles.

(2) The form error was more sensitive to the feed-direction wheel setting error than the lateral wheel setting error during the grinding of large-diameter aspherical surfaces. In addition, the form error in the central region was more sensitive to the wheel setting error in the axial direction of the grinding wheel than that in the tangential direction.

(3) The maximum form error induced by the feed-direction setting error was recorded at the rim of the workpiece. It exhibited a bilinear relationship with the wheel setting error and the distance to the optical axis. By contrast, the maximum form error caused by the lateral wheel setting error was recorded at the center of the workpiece.

(4) Based on the relationship between the wheel setting error and form error, the setting error was determined and used to accurately align the wheel during the grinding tests. An error compensation method integrating tilt correction, filtering, and partial

compensation was proposed to efficiently reduce the form error. The results showed that a form error of 3.4 μm PV was achieved for a Φ400 mm elliptical K9 glass surface.

Acknowledgements
Not applicable.

Authors' contributions
CL was in charge of the theoretical analysis, experiments and manuscript writing. LS took part in the experimental design and grinding tests. ZC and JC participated in measuring the workpiece form error. QL, JD and ZJ assisted with the modeling and data analysis. All authors read and approved the final manuscript.

Authors' Information
Changsheng Li, born in 1989, is currently an assistant professor at *School of Mechanical Engineering, Xi'an Jiaotong University, China*. He received his BSc, MSc and Ph.D. from *Xi'an Jiaotong University, China*, in 2012, 2015 and 2019. His research interests include precision/ultra-precision machining and precision assembly.
Lin Sun, born in 1989, is currently an assistant professor at *School of Mechanical Engineering, Xi'an Jiaotong University, China*. He received his BSc in *Northeastern University, China*, in 2012, and Ph.D. degree in ultra-precision grinding from *Xi'an Jiaotong University, China*, in 2019.
Zhaoxiang Chen, born in 1988, is currently an assistant engineer and a master candidate at *State Key Laboratory for Manufacturing Systems Engineering, Xi'an Jiaotong University, China*. He received his BSc in mechanical engineering from *Politecnico di Torino, Italy*, in 2013.
Jianfang Chen, born in 1985, is currently an engineer at *Shaanxi Qinchuan Precision CNC Machine Tool Engineering Research Co., China*.
Qijing Lin is currently an associate research fellow at *School of Mechanical Engineering, Xi'an Jiaotong University, China*. He received his BSc, MSc and Ph.D. degree from *Xi'an Jiaotong University, China*. His research interests include micro-/nano-fabrication and micro-/nano- sensors.
Jianjun Ding is currently a professor at *School of Mechanical Engineering, Xi'an Jiaotong University, China*. He received his BSc and MSc degree from *Central South University, China*, and Ph.D. degree from *Xi'an Jiaotong University, China*.
Zhuangde Jiang is a distinguished professor in the field of MEMS, nanotechnology and precision engineering. He is an academician of *Chinese Academy of Engineering* and a professor at *Xi'an Jiaotong University*, *China*. In addition, Professor Jiang is affiliated with a number of committees at national levels. He is the director of *Strategic Steering Committee under the State Council*, the Head of Mechanical Discipline Assessment of *National Science and Technology Award Committee*, Vice Chairman of *Chinese Society of Micro-Nano Technology*, and the President of *Shaanxi Provincial Association of Science and Technology*.

Funding
Supported by Fellowship of China National Postdoctoral Program for Innovative Talents (Grant No. BX20200268), Research Project of State Key Laboratory of Mechanical System and Vibration (Grant No. MSV202103), National Natural Science Foundation of China (Grant No. 51720105016), and Higher Education Discipline Innovation Project (Grant No. B12016).

Competing Interests
The authors declare no competing financial interests.

Author Details
[1]State Key Laboratory for Manufacturing Systems Engineering, Xi'an Jiaotong University, Xi'an 710049, China. [2]School of Mechanical Engineering, Xi'an Jiaotong University, Xi'an 710049, China. [3]Shaanxi Qinchuan Precision CNC Machine Tool Engineering Research Co, Xi'an 710018, China.

Received: 4 January 2021 Revised: 7 July 2021 Accepted: 11 July 2022
Published online: 14 August 2022

References

[1] J H Campbell, R A Hawley-Fedder, C J Stolz, et al. NIF optical materials and fabrication technologies: an overview. *Proceedings of SPIE's Lasers and Applications in Science and Engineering*, 2004: 5341.
[2] P Gray, E Ciattaglia, C Dupuy, et al. E-ELT assembly, integration, and technical commissioning plans. *Proceedings of SPIE's Astronomical Telescopes+ Instrumentation*, 2016, 9906: 99060X.
[3] D Schneider. Where no one has seen before: The James Webb Space Telescope will let us see back almost to the big bang. *IEEE Spectrum*, 2021, 58(1): 30-31.
[4] Y Fujii, T Uno, S Ariki, et al. Experimental study of 3.6-meter segmented-aperture telescope for geostationary Earth observation satellite. *Proceedings of SPIE's International Conference on Space Optics - ICSO 2021*, 2021, 9145: 91452F.
[5] E Miao, S Gao, J Zhang, et al. Sub-nanometer asphere fabrication and testing. *Proceedings of SPIE's Eighth International Symposium on Advanced Optical Manufacturing and Testing Technology (AOMATT2016)*, 2016, 9684: 96840H.
[6] T Usuda, Y Ezaki, N Kawaguchi, et al. Preliminary design study of the TMT telescope structure system: overview. *Proceedings of SPIE's Astronomical Telescopes+ Instrumentation*, 2014, 9145: 91452F.
[7] J-L Miquel, D Batani, N Blanchot. Overview of the laser mega joule (LMJ) facility and PETAL project in France. *The Review of Laser Engineering*, 2020, 42(2): 131.
[8] Z Zhang, X Yang, L Zheng, et al. High-performance grinding of a 2-m scale silicon carbide mirror blank for the space-based telescope. *The International Journal of Advanced Manufacturing Technology*, 2017, 89(1): 463-473.
[9] C J Oh, A Lowman, G Smith, et al. Fabrication and testing of 4.2m off-axis aspheric primary mirror of Daniel K. Inouye Solar Telescope. *Proceedings of SPIE's Astronomical Telescopes + Instrumentation*, 2016, 9912: 99120O.
[10] [10] M Feng, Y Wu, Y Wang, et al. Investigation on the polishing of aspheric surfaces with a doughnut-shaped magnetic compound fluid (MCF) tool using an industrial robot. *Precision Engineering*, 2020, 61: 182-193.
[11] Y Wang, C Dai, W Li, et al. Polishing an off-axis aspheric mirror by ion beam figuring. *Proceedings of SPIE's Eighth International Symposium on Advanced Optical Manufacturing and Testing Technology (AOMATT2016)*, 2016, 9683: 96830H.
[12] C Li, X Li, S Huang, et al. Ultra-precision grinding of Gd3Ga5O12 crystals with graphene oxide coolant: Material deformation mechanism and performance evaluation. *Journal of Manufacturing Processes*, 2021, 61: 417-427.
[13] R E Parks, P Lam, W Kuhn. The large optical generator: a progress report. *Proceedings of SPIE's 1985 Albuquerque Conferences on Optics*, 1985, 0542: 28-31.
[14] H M Martin, R G Allen, J H Burge, et al. Fabrication of mirrors for the magellan telescopes and the large binocular telescope. *Proceedings of SPIE's Astronomical Telescopes and Instrumentation*, 2003, 4837: 609-618.
[15] S West, H Martin, R Nagel, et al. Practical design and performance of the stressed-lap polishing tool. *Applied Optics*, 1994, 33(34): 8094-8100.
[16] P Shore, P Parr-Burman. Manufacture of large mirrors for ELTs: a fresh perspective. *Proceedings of SPIE's Optical Systems Design*, 2004, 5252: 55-62.
[17] P Shore, P Morantz, X Luo, et al. Big OptiX ultra precision grinding/measuring system. *Proceedings of SPIE's Optical Systems Design*, 2005, 5965: 59650Q.
[18] P Comley, P Morantz, P Shore, et al. Grinding metre scale mirror segments for the E-ELT ground based telescope. *CIRP Annals-Manufacturing Technology*, 2011, 60(1): 379-382.
[19] Z Zhang, R Li, L Zheng, et al. Precision grinding technology for the off-axis aspherical silicon carbide mirror blank. *Journal of Mechanical Engineering*, 2013, 49(17): 39-45. (in Chinese)
[20] G Wang, S Li, Y Dai. Design method and accuracy analysis of aspherical optical compound machine tool. *China Mechanical Engineering*, 2004, 15(2): 99-102. (in Chinese)
[21] Z Xuejun, Z Yunfeng, Y Jingchi, et al. FSGJ 1 aspheres automatic fabrication and on line testing system. *Optics and Precision Engineering*, 1997, 5(2): 70-76. (in Chinese)

[22] Z Feng, F Di, L Ruigang, et al. Fabrication and testing of aspheric silicon carbide mirror. *Journal of Applied Optics*, 2008, 29(6): 1004-1008. (in Chinese)
[23] L Bin, X Jianpu, R Dongxu, et al. Compensation grinding and independent on-machine measurement of symmetric aspheric mirror. *Manufacturing Technology and Machine Tool*, 2019, (2): 129-134.
[24] J P Xi, H Y Zhao, B Li, et al. Profile error compensation in cross-grinding mode for large-diameter aspheric mirrors. *The International Journal of Advanced Manufacturing Technology*, 2016, 83(9): 1515-1523.
[25] X Long, P Zhao, J Ding, et al. Optimal design and simulation of the stepped beam of a large-scale ultra-precision optical aspheric machine. *International Journal of Nanomanufacturing*, 2017, 13(3): 210.
[26] X Wei, B Li, L Chen, et al. Tool setting error compensation in large aspherical mirror grinding. *The International Journal of Advanced Manufacturing Technology*, 2018, 94(9): 4093-4103.
[27] Y Wang, C Zhang, Y He, et al. Development and evaluation of non-contact automatic tool setting method for grinding internal screw threads. *The International Journal of Advanced Manufacturing Technology*, 2018, 98(1): 741-754.
[28] S Maeng, S Min. Simultaneous geometric error identification of rotary axis and tool setting in an ultra-precision 5-axis machine tool using on-machine measurement. *Precision Engineering*, 2020, 63: 94-104.
[29] G Zhang, Y Dai, Z Lai. A novel force-based two-dimensional tool centre error identification method in single-point diamond turning. *Precision Engineering*, 2021, 70: 92-109.
[30] W Gao, Y-L Chen, K-W Lee, et al. Precision tool setting for fabrication of a microstructure array. *CIRP Annals*, 2013, 62(1): 523-526.
[31] J Dai, H Su, T Yu, et al. Experimental investigation on materials removal mechanism during grinding silicon carbide ceramics with single diamond grain. *Precision Engineering*, 2018, 51: 271-279.
[32] Y Wang, Y Geng, G Li, et al. Study of machining indentations over the entire surface of a target ball using the force modulation approach. *International Journal of Extreme Manufacturing*, 2021, 3(3): 035102.
[33] Y Cheng, H Yu, Z Yu, et al. Imaging analysis of micro-milling tool in the process of tool setting based on digital holography. *IEEE International Conference on Manipulation, Manufacturing and Measurement on the Nanoscale (3M-NANO)*, 2019: 33-36.
[34] F Chen, S Yin, H Huang, et al. Fabrication of small aspheric moulds using single point inclined axis grinding. *Precision Engineering*, 2015, 39: 107-115.
[35] N Kang, S Li, Z Zheng. Research on geometric model of grinding large and medium scales optical aspheric surfaces. *Proceedings of SPIE's ICO20: Optical Devices and Instruments*, 2006, 6034: 60341B.
[36] X H Lin, Z Z Wang, Y B Guo, et al. Truing error analysis of arc wheel in optical aspheric grinding. *Acta Armamentarii*, 2013, 34(1): 60-65. (in Chinese)
[37] X H Lin, Z Z Wang, Y B Guo. Development and application of cup truer in advanced optical grinding. *Diamond Abrasives Engineering*, 2009, (1): 18-22. (in Chinese)